Liquid Phase Modeling in Porous Media: Adsorption of Methanol and Ethanol in H-MFI in condensed water

Subrata Kumar Kundu, Muhammad Zeeshan, Panuwat Watthaisong, and Andreas Heyden*

Department of Chemical Engineering, University of South Carolina

301 South Main Street, Columbia, SC 29208, USA.

*Corresponding author: email: heyden@cec.sc.edu

ABSTRACT

Zeolites are used in the chemical and separation industries for their exceptional selectivity, adsorption capacity, regenerability, and stability in gas and liquid phase processing. Here, we developed an explicit solvation method for predicting solvent/condensed phase effects on adsorption free energies in microporous media such as zeolites based on the hybrid quantum mechanical/molecular mechanical free energy perturbation (QM/MM-FEP) technique. Our explicit solvation method for zeolite systems, called eSZS, aims to capture site-specific interactions during the adsorption process at the Brønsted acid sites of H-MFI zeolite while still considering the diverse configuration space of the solvent molecules. This strategy is ideal for chemical reactions or adsorbates that interact with the microporous medium in few distinct adsorbate/transition state configurations, i.e., the harmonic or similar approximations are acceptable for the adsorbate/transition state while such approximations break down for the solvent molecules that require extensive configuration space sampling. In this way, our approach effectively overcomes the limitations of implicit solvation models and classical force field methods for describing solvation effects on chemical reactions within porous materials such as zeolites. Specifically, in this study, we investigated various aspects of our hybrid QM/MM approach, including QM cluster size dependencies in a periodic electrostatically embedded cluster model (PEECM), rules for link atoms at the QM/MM boundary, and functional and basis set considerations for converged and reasonably accurate gas and aqueous phase methanol and ethanol adsorption free energy predictions in H-MFI. For gas phase adsorption of methanol and ethanol in H-MFI at a Brønsted acid site in T12 position, we compute adsorption free energies at 298 K of -0.61 eV and -0.75 eV, respectively, using a

PEECM containing 50 Si and 1 Al atom with ωB97x-D/def2-TZVP level of theory. For solvent effect calculations, we sample the aqueous phase using grand canonical Monte Carlo (GCMC) simulations to (1) obtain a mean field of electrostatic interactions in the reaction system and (2) perform a rigorous free energy perturbation calculation. Similar to the experimentally and computationally observed endergonic solvation effects observed for hydrocarbon adsorption on metal surfaces, we also observe that a condensed aqueous environment destabilizes methanol and ethanol at these acid sites in H-MFI at 298 K. Specifically, the computed solvation free energies of adsorption ($\Delta\Delta G_{solv}$) for methanol and ethanol are +0.44 eV and +0.54 eV, respectively. From this study, it is evident that adsorbates (methanol and ethanol) are competing with water for adsorption space inside the H-MFI zeolite, leading to an endergonic solvation effect. We expect that the endergonic, aqueous solvent effect during adsorption in microporous zeolites is highly tunable by changing the pore size and hydrophobicity of the microporous material as this will affect the water density inside the pore structure.

2. INTRODUCTION

Understanding adsorption and desorption of molecules in and out of hydrophilic and hydrophobic zeolites in the presence of solvents is essential for improving wastewater purification, catalysis, and separation technologies.[1,2] Solvents such as liquid water affect the thermodynamics, rate, and selectivity of adsorption without being engaged in chemical transformations.[3] Both the adsorbate and adsorption site, e.g., the Brønsted acid site in a zeolite, are affected by the solvent interactions, and it is difficult to predict the solvent influence on adsorption and desorption of a complex adsorbate in a porous zeolite framework.[4] Zeolite materials are one of the most important proton-exchanged acid-base catalysts in the petrochemical industry because of their well-defined active sites and microporous structure.[5-9] Structurally, zeolites are made of corner-sharing tetrahedrally coordinated silicate (SiO_4) units, where the substitution of Si atoms by Al atoms induces a negative charge in the framework that is charge-balanced by cations, such as protons (H^+).These protons (H^+) bond to framework oxygen, which is coordinated to tetrahedral Al, thereby rendering the zeolite framework hydrophilic. Adsorption and chemical reaction occurring inside the complex zeolite micropores are challenging to understand and model in the presence of solvent molecules because of the non-uniform distribution of solvent molecules inside the zeolite pores. A few research studies used IR and NMR spectroscopies, temperature-programmed desorption, and microcalorimetry to investigate zeolite acidity, adsorption capacity, and adsorption energies in vapor phase and from solution.[10-20] In addition, adsorption, diffusion, and chemical reactions in zeolites can be studied by molecular simulations, filling the gaps not covered by experiments.[21,22] For example, several computational studies ranging from electronic structures calculations,

84 molecular dynamics and Monte Carlo simulations have revealed catalytic activity,
85 adsorption, and diffusion trends.[23-25] Specifically of relevance to this study, researchers
86 have investigated water adsorption in hydrophilic and hydrophobic zeolites of FAU, MFI,
87 MOR structure (different Si/Al ratio) by force field-based Grand Canonical Monte Carlo
88 (GCMC) simulations, with an emphasis on describing and understanding the cation
89 adsorption sites and their sensitivity to force field parameters.[26-30]

90 To model reactions in the zeolite micropores, density functionals with empirical or
91 semi-empirical corrections are typically used, as there are no reliable force fields available
92 that can describe chemical reactions.[31,32] However, due to the large size of the periodic
93 zeolite structure, only a cluster of the zeolite framework is often described at the DFT
94 level.[33-37] While periodic DFT calculations—that can consider the long-range interactions
95 in these systems have been performed for small zeolite unit cells, they are often limited to
96 generalized gradient approximation (GGA) functionals that are not ideal for describing the
97 interactions in insulators such as zeolites.[38,39] We note that the computational time
98 requirements increase significantly with an increasing number of water molecules and
99 zeolite atoms in the simulation system needed to capture the dispersive and electrostatic
100 interactions.

101 The use of quantum mechanical/molecular mechanical models of the extended
102 zeolite framework surrounding the active sites has also been practiced. In this study, we
103 modeled an extended zeolite framework via hybrid quantum mechanical/molecular
104 mechanical (QM/MM) simulations in vapor and condensed aqueous phases. Zeolite cluster
105 models are subdivided into two regions: a reactive portion consisting of the active site and
106 the adsorbate, which is described by DFT/QM, and an inactive region – which includes the

zeolite framework atoms and the water molecules that are described by a molecular mechanics (MM) force field. This hybrid QM/MM scheme is computationally far more efficient than a pure DFT description and, hence, ideally suited for studying large zeolite frameworks in the presence of water molecules. We note that bond-breaking and/or bond-formation are described at the DFT or QM level of theory while other crucial but distant interactions, such as the long-range electrostatic and dispersion interactions of water molecules and zeolite framework atoms, are captured through force fields. Notably, the effect of the long-range electrostatic interactions on the electronic structure calculation can also be considered. Nevertheless, concerns remain about how large a zeolite framework cluster should be included in the QM/MM simulations (containing "liquid" water molecules) to obtain converged simulation results. Similarly, uncertainties persist about the optimal correlation functional and basis set[40-44] and which charge and Lennard-Jones parameters can successfully capture the interactions within the adsorbate-zeolite-water system.

In this work, we have developed a hybrid quantum mechanical and molecular mechanical (QM/MM) approach with electrostatic embedding to investigate the adsorption of two model molecules – methanol and ethanol from liquid water at the T12 acid site in H-MFI zeolite. Adsorption at the Brønsted acidic site of H-MFI from liquid water is demonstrated to be sensitive to small changes in the force field parameters, water model, framework atom positions, and zeolite atom partial charges, highlighting the need for this study. To study the effect of liquid water on the adsorption properties of methanol and ethanol at the T12 site in H-MFI, we identified a computationally efficient thermodynamic cycle and performed free energy perturbation (FEP) calculations that directly compute the

free energy of solvation ($\Delta\Delta G_{solv}$) for adsorbed states (or in principle transition states) in a porous zeolite structure.

3. COMPUTATIONAL METHODS

3.1 Gas Phase Adsorption

Overall, we adopt a QM/MM description of our zeolite system in which the long-range electrostatic interactions of distant atoms affecting the QM system are considered at the electrostatically embedded DFT level. Specifically, the crystallographic MFI structure was used to determine the positions of atoms in the zeolite models.[45-47] The T12 site in MFI is the most energetically favorable site for replacing Si with Al, hence this site was chosen for subsequent calculations.[46,47] By substituting a Si atom with an Al atom in the T12 site, an acidic site is created, i.e., the resulting charge is balanced by a proton/hydrogen (H) atom on the oxygen atom connected to the Al atom.

We proceeded with four different zeolite clusters containing 5, 26, 51, and 90 tetrahedral atoms. These clusters represent the QM subsystem in our QM/MM model, named T5, T26, T51, and T90, and were cut from a larger periodic supercell of H-MFI that had unit cell dimensions of 40.1399 Å × 39.8400 Å × 26.8400 Å. To stabilize the clusters, the terminal oxygen atoms in each cluster were replaced with hydrogen atoms. Specifically, we replaced each terminal Si-O bond with a single hydrogen link atom. The terminal hydrogen atoms were positioned at a distance of 0.92 times the Si-O bond length (approximately 1.47 Å) from the terminal Si atom.[48] This arrangement helped remove any uncoordinated Si fragments. During the geometry optimization of each cluster, the coordinates of the terminal H atoms and the Si atoms attached to them were kept constant. Figure 1 illustrates the clusters used in this paper. Finally, to maintain the electrostatic

neutrality of the MM subsystem, we adjusted the charges for the subset of terminal atoms of the MM system as described in section 4.2.

Two different range-separated hybrid GGA and meta hybrid GGA functionals with dispersion corrections, namely ωB97-D and ωB97x-D, were employed for the geometry optimizations. Also, two different basis sets were used: the split valence with polarization functions def2-SV(P) and the triple-ζ basis with valence polarization functions def2-TZVP. These calculations were carried out using the TURBOMOLE 7.5 software.[49-51]

Peng Bai et al. demonstrated that the standard TraPPe-zeo force field, which includes Lennard-Jones and charge parameters, is capable of accurately predicting the adsorption and diffusion behavior of alkanes, alcohols, carbon dioxide, and water within all-silica zeolites over a wide range of temperatures and pressures.[48] This suggests that this force field is also well-suited for describing the behavior of zeolitic silicon and oxygen atoms in the MM subsystem of our QM/MM calculations as long as the QM subsystem is sufficiently large. We note that Bell et al. had to adjust their charge and Lennard-Jones parameters in their QM/MM model since they aimed to use a very small (T5) QM subsystem.[52-53] Given that our model also needs to describe the presence of water molecules in the pore structure (see section 3.2), we aimed to minimize any changes to the force field parameters and instead elected to use larger QM subsystems. The details of the force field and its validation are further discussed in section 4.2. Briefly, classical electrostatic and Lennard-Jones interactions are given by equation (1) and (2)–

$$E_{elec} = \sum_{ij} \frac{q_i q_j}{4\pi\epsilon_0 r_{ij}} \quad (1)$$

$$E_{LJ} = \sum_{ij} 4\varepsilon_{ij} \left[\left(\frac{\sigma_{ij}}{r_{ij}} \right)^{12} - \left(\frac{\sigma_{ij}}{r_{ij}} \right)^{6} \right] \quad (2)$$

where $\varepsilon_{ij} = (\varepsilon_i \varepsilon_j)^{1/2}$, $\sigma_{ij} = (\sigma_i + \sigma_j)/2$, q_i is atomic partial charge, σ_i is the size parameter of atom *i*, and ε_i is the potential well depth of the Lennard-Jones potential for atom *i*. For adsorbate atoms, standard OPLS-AA Lennard-Jones parameters were used.[54] Thus, the total energy of our periodic electrostatically embedded QM/MM system, $E_T(r_{QM}, r_{MM})$, becomes [55]–

$$E_T(r_{QM}, r_{MM}) = \langle\psi|\, H_{eff}(r_{QM},\, r^o_{MM})|\psi\rangle + \left\{\left[E^{elec+vdW}_{MM+QM/MM}(r_{QM}, r^o_{MM})\right]_{Q_i=0, i\in QM} - \left[E^{elec+vdW}_{MM+QM/MM}(r_{QM}, r^o_{MM})\right]\right\} + E^{elec+vdW}_{MM+QM/MM}(r_{QM}, r_{MM}) \quad (3)$$

where r_{QM} symbolizes the QM cluster atom coordinates that are embedded in MM atoms (r_{MM}) represented by point charges and Lennard Jones interaction sites. Here, r^o_{MM} represents a set of reference MM atom coordinates (in the gas phase scenario, these are simply the MM zeolite atoms, but we select this nomenclature to facilitate understanding the liquid phase scenario), $\langle\psi|\, H_{eff}(r_{QM},\, r^o_{MM})|\psi\rangle$ symbolizes a periodic electrostatically embedded DFT calculation in the periodic point charge field of the MM reference atoms. $\left[E^{elec+vdW}_{MM+QM/MM}(r_{QM}, r^o_{MM})\right]_{Q_i=0, i\in QM}$ symbolizes the electrostatic and van-der-Waals interactions among the (reference) MM atoms and the van-der Waals interactions between the (reference) MM and QM atoms. Finally, $E^{elec+vdW}_{MM+QM/MM}(r_{QM}, r^o_{MM})$ and $E^{elec+vdW}_{MM+QM/MM}(r_{QM}, r_{MM})$ represent the classical van-der-Waals and electrostatic interactions in the total system at reference MM and general MM coordinates, respectively. In the absence of solvent, the MM zeolite coordinates remain unchanged, i.e., the reference MM and general MM coordinates are the same, and the last two terms cancel (unlike in the situation described in the next section). Otherwise, we use the fixed charge approximation

when optimizing the QM cluster coordinates.[56] In summary, for gas phase zeolitic adsorption, only one MM conformer is present and equation (3) simplifies to–

$$E_T(r_{QM}, r_{MM}) = \langle\psi|\, H_{eff}(r_{QM},\, r^{o}_{MM})|\psi\rangle + \left[E^{elec+vdW}_{MM+QM/MM}(r_{QM}, r^{o}_{MM})\right]_{Q_i=0, i\in QM} \quad (4)$$

Next, the self-consistent field (SCF) energy convergence criterion is set to 10^{-7} Ha (Hartree), and a Gauss-Chebyshev-type spherical grid, m4, is used for numerical integrations. Optimizations are considered converged when the maximum norm of the cartesian gradient is smaller than 10^{-3} Ha bohr^{-1}.

To compare our QM/MM results to periodic QM(high level of theory)/QM(periodic low level of theory) data that are presumably more accurate, we adjusted the optimized cluster atom coordinates (optimized with high-level functionals) in a periodic zeolite supercell (1×1×2) and used the Vienna Ab Initio Simulation Package (VASP) to perform single-point calculations of the whole periodic system, i.e., we solved the Kohn-Sham equations under periodic boundary conditions and obtained VASP adsorption energies, QM (periodic low level of theory).[57-58] Here, we used the projector-augmented wave method (PAW) to model electron-ion interactions with the Perdew-Burke-Ernzerhof (PBE-D3) functional to describe exchange and correlation. Due to the large size of the simulation system, we performed only gamma point calculations according to the Monkhorst-Pack scheme with a Methfessel-Paxton smearing of 0.2 eV.[59-63] We set the energy cut-off to 520 eV for the plane waves in the calculations, and we used a self-consistent field (SCF) energy convergence criterion of 10^{-7} eV. The QM/QM approach can be understood as either correcting the limitations of the PBE-D3 functional with higher level cluster calculations or as correcting high level QM/MM calculations for cluster size limitations. Ultimately, it

is a subtractive ONIOM-like scheme similar to what is done by Sauer et al.[38,64] The main difference between our and Sauer's approach is that our cluster calculations are embedded in a periodic point charge field while such a field is not present by Sauer et al. Importantly, both QM/QM approaches do not utilize any Lennard Jones force field parameters and the energy becomes:

$$\Delta E_{\text{High level :Low level}}(\text{periodic, cluster}) = \Delta E_{\text{High level}}(\text{cluster}) + \Delta E_{\text{Low level (PBE-D3)}}(\text{periodic}) - \Delta E_{\text{Low level (PBE-D3)}}(\text{cluster}) \quad (5)$$

Finally, for the free energy calculations of an adsorbed species, we used the modified rigid rotor-harmonic oscillator approach (quasi-RRHO)[65] applied to the high level of theory cluster model potential energy surface (it is not computationally practical to compute all frequencies at the periodic DFT level of theory) –

$$A\left[\frac{J}{\text{moles}}\right] = -k_B T\left[\ln\left\{\left(\frac{2\pi m k_B T}{h^2}\right)^{3/2}\frac{k_B T}{P}\right\} + 1 + \left(1 - \omega(\nu_j)\right) \times \frac{1}{2}\ln\left(\frac{T}{\theta_r}\right) + \omega(\nu_j) \times \sum_{j=1}^{3N-6(5)}\left(-\frac{\theta_{\nu_j}}{2T} - \ln\left(1 - \exp\left(-\frac{\theta_{\nu_j}}{T}\right)\right)\right) + \ln \omega_{e1} - \frac{E_{Ads}}{k_B T}\right] \quad (6)$$

$$\omega(\nu_j) = \frac{1}{1+\left(\frac{\nu_0}{\nu_j}\right)^4} \quad (7) \qquad \theta_{\nu_j} = \frac{h\nu_j}{k_B} \quad (8) \qquad \theta_r = \frac{h^2}{8\pi^2 \mu_{corr} k_B T} \quad (9)$$

Here, ν_j are wave numbers within the harmonic approximation, ν_0 is chosen as 100 cm^{-1}, T is the absolute temperature, k_B is the Boltzmann constant, μ_{corr} is the corrected moment of inertia where $\mu_{corr} = \mu B_{av}/(\mu + B_{av})$, $\mu = h/(8\pi^2 \nu_j)$, and B_{av} (= average molecular moment of inertia) = 10^{-44} kg m^2 is given in reference 71. We note that using the corrected moment of inertia, μ_{corr}, versus μ, leads to negligible changes in θ_r of smaller

1% for frequencies larger 3 cm^{-1}. Next, the enthalpy of adsorption, $\Delta H = \Delta A + T\Delta S$, is computed from the free energy and a weighted entropy.[65]

$$S = \left\{\omega(\nu_j) \times \text{vibrational entropic contribution}(S_v) + \left(1 - \omega(\nu_j)\right) \times \text{low frequency mode entropic contribution } (S_R)\right\} \quad (10)$$

3.2 Liquid Phase QM/MM Simulation Details

Ultimately, we are interested in the effect of condensed water in the zeolite pores on the adsorption behavior of hydrocarbons at low concentration. In the liquid phase, water adsorption isotherms in microporous zeolite were calculated using grand-canonical, μVT, Monte Carlo simulations. The computation involved different types of Monte Carlo moves: molecule insertion and deletion (50% of moves), molecule translation (25%), and molecule rotation (25%). This approach was also employed for determining chemical potentials related to the bulk phase by introducing water molecules into a box at 298 K and identifying the phase transitions. We used the open-source Monte Carlo Cassandra v1.2.4 package for these simulations.[66,67] All guest-host (water–zeolite) interactions were truncated at r_{cut} = 12 Å, and tail corrections were used to estimate the Lennard Jones (LJ) interactions beyond the cut-off. During liquid phase simulations, zeolite framework atoms were represented as rigid, and zeolite-adsorbate-water and/or zeolite-water interactions were based only on the water molecule placement, i.e., for each Monte Carlo simulation not only the zeolite atoms but also the adsorbate atoms where fixed. In other words, we used the rigid rotor-harmonic oscillator approximation for the adsorbate and zeolite atoms and only sampled the water molecules. As described below, the QM zeolite – adsorbate

cluster is optimized in the mean field of the water molecules and distant zeolite atoms. Here, we used the fixed partial charge approximation on atomic centers and computed electrostatic energies using Ewald summations with a real space cutoff of 12 Å and an accuracy of 10^{-5}.

We used the TIP4P/2005 water model for studying water adsorption within the H-MFI zeolite. Abascal et al. demonstrated that the TIP4P/2005 four-site model outperforms TIP3P, SPC/E, and TIP5P in predicting compressibility, expansivity, heat capacity behavior within dense regions of the phase diagram, melting properties, and phase diagram characteristics across a wide temperature range (123 K to 573 K) and pressures up to 40,000 bar.[68] While more accurate water potentials such as MB-pol are available,[69] these potentials can often not be used together with the potential parameters for zeolites or hydrocarbons, explaining why, for many QM/MM-FEP applications, the TIP4P/2005 water model is preferred.

Our research group has previously developed an explicit solvation scheme for metal surfaces (eSMS), incorporating the QM/MM-FEP (quantum mechanics/molecular mechanics-free energy perturbation) approach with NVT molecular dynamics simulations for heterogeneous metal catalysis problems.[70-72] Very good agreement with experimental solvation free energies could be obtained for phenol, benzene, and furfural adsorption on Pt(111), highlighting the accuracy and practicability of the QM/MM-FEP approach for solid-liquid interface modeling.[73, 74] This QM/MM-FEP-based explicit solvation package was successfully employed here after necessary modifications described below to carry out free energy calculations in electronically isolating (non-conductive) zeolite systems. Key modifications have been a change in the energy function (see Equation 11 below) and

implementing a sampling approach of the water molecules within the zeolite under a μVT ensemble, where the number of water molecules can differ in each configuration. We note that the change in energy function is likely only possible for electronically non-conductive systems, while the change to a μVT ensemble and Monte Carlo sampling is likely critical for all porous systems that cannot be efficiently sampled by molecular dynamics simulations. To determine free energy differences between two states, we employed the Bennett acceptance ratio (BAR), which offers enhanced efficiencies compared to exponential averaging when dealing with two sampled states, utilizing both the forward and reverse distributions.[75] The free energy estimation process was repeated by three independent simulations, each comprising 100 million Monte Carlo (MC) steps with distinct random seeds. This generated independent trajectories, and average properties (specifically, the overall free energy) and 95% confidence intervals of the overall free energy were computed from these three independent estimations of the free energy of adsorption in zeolite in the presence of water.

In the following, we describe our thermodynamic cycle and the individual steps for computing solvation effects on adsorption free energies in zeolites in detail. We call our approach explicit solvation method for zeolite systems (eSZS). Figure 2 illustrates a visual representation of our free energy calculation. We highlight that the high efficiency of our thermodynamic cycle and overall approach hinges on the accuracy of our QM/MM potential and the ability to treat the QM atom coordinates by the quasi-RRHO approach and only sampling the MM part of the simulation system. This approximation is likely excellent for most inorganic systems and catalysts whenever the adsorbate interacts strongly with the active site.

The total energy function for the explicit solvation approach is defined as:

$$E_T\left(\underline{r}_{QM}, \underline{r}_{MM\ Zeo+MM\ Water}\right) = \langle \Psi \left| H_{eff}\left(\underline{r}_{QM}, \underline{r}^{MeanField(100)}_{MM\ Zeo\ +\ MM\ Water}\right)\right| \Psi\rangle +$$

$$\frac{1}{100}\sum_{j=1}^{100}\left\{\left[E^{elec+vdW}_{j,(MM\ Zeo\ +\ MM\ Water)\ +QM/(MM\ Zeo\ +\ MM\ Water)}\left(\underline{r}_{QM}, \underline{r}^{MeanField(100)}_{MM\ Zeo\ +\ MM\ Water}\right)\right]_{Q_i=0, i\in QM} - \right.$$

$$\left. E^{elec+vdW}_{j,(MM\ Zeo\ +\ MM\ Water)+QM/(MM\ Zeo\ +\ MM\ Water)}\left(\underline{r}_{QM}, \underline{r}^{MeanField(100)}_{MM\ Zeo\ +\ MM\ Water}\right)\right\} +$$

$$E^{elec+vdW}_{j,(MM\ Zeo\ +\ MM\ Water)\ +QM/(MM\ Zeo\ +\ MM\ Water)}\left(\underline{r}_{QM}, \underline{r}_{MM\ Zeo\ +\ MM\ Water}\right) \quad (11)$$

Equation 11 is essentially equivalent to equation 3 for the gas-phase system. The only difference is that the DFT calculations are performed in a mean-field of, in this case, one hundred independent water conformations (charges scaled by one hundredth). The first two terms describe the system energy in a mean-field of water molecules. The third term subtracts the classical electrostatic and van-der-Waals interactions of the mean-field reference configurations, and the fourth term adds the classical electrostatic and van-der-Waals interactions of an actual water configuration. A key difference to our previous eSMS method for metal surfaces is that only one DFT calculation must be performed to compute the system energy, while three DFT calculations are required in standard eSMS calculations – one additional plane wave DFT gas phase calculation and another gas phase cluster calculation are necessary for standard eSMS.[70-73] The other DFT calculations in standard eSMS of metal systems result from the difficulty in defining a meaningful QM/MM description of a metal surface. In contrast, for an insulating material such as a zeolite, QM/MM descriptions are more straightforward, and the energy difference between the extra plane wave DFT calculation and the extra gas phase cluster calculation is small for energy difference calculations such that these terms can be neglected.

As shown in Figure 2, State $1_{opt,0}$ consists of a liquid-phase optimized zeolite-adsorbate system and a second gas-phase optimized zeolite system. State 5 consists of a liquid-phase optimized zeolite system without adsorbate and a second gas-phase optimized zeolite system with the adsorbate in the gas phase. Thus, the energy difference between State $1_{opt,0}$ and State 5 is the free energy of adsorption for a gas molecule adsorbing in a zeolite filled with water (the two gas phase zeolite system energies cancel but are still important for the intermediate steps).

State $1_{opt,0}$ to State 1: Practically, our solvation effect calculation starts with gas-phase optimized structures of the adsorbate-zeolite system with and without adsorbate and with and without water (State 1). Thus, we first compute the free energy difference between $1_{opt,0}$ and 1_{opt} which consists of the same liquid phase optimized system as $1_{opt,0}$ and the gas phase optimized system with adsorbate in which the adsorbate was removed, i.e., the free energy difference between state $1_{opt,0}$ to state 1_{opt} is computed by two single gas-phase energy calculations (no sampling is necessary). Next, from state 1_{opt} to state 1, the liquid phase system transitions from liquid-phase optimized coordinates to gas-phase optimized zeolite and adsorbate coordinates. Given that the mean-field ensemble changes during the transition of liquid-phase optimized coordinates to gas-phase optimized coordinates, intermediate states are introduced for the FEP calculation of this transition. The gas-phase subsystem is not changing during this transition.

State 1 to State 2: Between State 1 and 4, the zeolite atom coordinates and adsorbate coordinates do not change, except that in State 1, the adsorbate is in the liquid subsystem while the adsorbate is in the gas-phase system in State 4. However, the charges and Lennard Jones parameters on the QM atoms change. Specifically, the charge and Lennard Jones

parameters of the adsorbate in the liquid phase subsystem disappear, along with changes in the charge parameters of the zeolite QM atoms. Both of these changes modify the mean water field. Thus, between State 1 and State 2, we linearly transition the partial charges of the QM atoms from those in State 1 to those in State 4. State 1a in Figure 2 is one of these intermediate states. Specifically, we derived the charges for the MM interaction energy between the water molecules and the quantum cluster and adsorbate from Natural Population Analysis (NPA).[76] We note that during the transition from State 1 to State 2, all energy terms in equation 11, but the last, remain unchanged such that the free energy calculation between State 1 and State 2 does not involve any DFT calculation. Instead, this transition is computed using conventional classical FEP calculations that only consider the change in mean water field due to changing the classical electrostatic interaction sites on the QM atom coordinates.

State 2 to State 3: Ultimately, the adsorbate must transition from the liquid-phase DFT calculation/subsystem to the gas-phase DFT calculation/subsystem. This free energy difference is computed between State 2 and State 3 and is essentially the "non-classical" contribution of solvent molecules changing the quantum system's electronic structure when transitioning from a zeolite-adsorbate system to one without adsorbate. This energy difference is the main difference between electrostatic and mechanical embedding of the QM/MM system. Practically, there cannot be intermediate states between State 2 and State 3, and the uncertainty in the free energy difference between these states (originating from modeling our mean water field from 100 water conformations) is reduced by using multiple independently determined mean water fields for State 1. We note that it can be argued that this transition should occur directly after State 1 (since it uses these water ensembles) but

to be consistent with our prior eSMS description,[73] we depict this energy difference after removal of the electrostatic interactions in our potential of mean force graphs.

State 3 to State 4: What remains is to remove the Lennard Jones interactions of the adsorbate in the liquid phase subsystem. This was accomplished using Shifted Lennard Jones (SLJ) potentials integrated into the Cassandra v1.2.4 open-source Monte Carlo package. The SLJ potential is defined by:

$$V_{SLJ} = (1-\lambda)\left[\frac{A}{(r^2+\delta\lambda)^6} - \frac{B}{(r^2+\delta\lambda)^3}\right] \quad (12)$$

where A ($= 4\varepsilon\sigma^{12}$) and B ($= 4\varepsilon\sigma^{6}$) are repulsive and attractive Lennard Jones parameters, respectively, r is the interatomic distance, δ is the shift parameter enabling a gradual transition of the Lennard Jones potential, and λ governs the smooth reduction of the van der Waals interaction strength (at $\lambda = 0$, the Lennard Jones interactions are fully present, at $\lambda = 1$ the Lennard Jones interactions are zero between the adsorbate and its environment, and for $0 < \lambda < 1$ the Lennard Jones potential smoothly diminishes). To ensure a smooth transition between an atom's presence in solution and its occupation of the cavity by solutes, the square of the van der Waals radius of the atom being phased out was utilized for the δ parameter, as proposed by Zacharias et al.[77] State 3a in Figure 2 is one of these intermediate states. Again, we note that during the transition from State 3 to State 4, all energy terms in equation 11, but the last, remain unchanged such that the free energy calculation between State 3 and State 4 does not involve any DFT calculation. Instead, this transition is computed using conventional, classical FEP calculations that only consider the change in mean water field due to changing the classical Lennard Jones interaction sites on the QM atom coordinates.

State 4 to State 4_{opt}: The zeolite coordinates of the QM cluster acquired from the zeolite-adsorbate vapor phase optimization transition to their optimized positions in water in the absence of adsorbate. This transition is synonymously to the transition from State 1 to 1_{opt} and involves a number of intermediate states for the FEP calculation as the mean water field ensemble changes significantly during this transition. The gas-phase subsystem is again not changing during this transition.

State 4_{opt} to State 5: Finally, we compute the desorption free energy for the gas-phase subsystem. The liquid phase subsystem remains unchanged here such that this computation is trivial. We note that we are assuming here that mass transfer in the liquid phase is fast and the adsorbate in liquid and gas are in equilibrium.

In summary, the steps outlined from state $1_{opt,0}$ to state 4_{opt} represent the solvent effect on the adsorption (or desorption) free energy of a gas phase adsorbate with a given fugacity into a porous medium filled by a solvent (here water).

4. RESULTS AND DISCUSSION

4.1 QM Cluster Size Dependency

Various cluster sizes and QM models were used to estimate the adsorption energies of methanol and ethanol in H-MFI. Figure 3 outlines the critical geometries that define the interaction of methanol with the Brønsted acid site in the H-MFI clusters. The adsorption energies for the QM clusters were computed using different range-separated hybrid GGA and hybrid meta-GGA functionals with dispersion corrections, specifically ωB97-D and ωB97x-D. Additionally, various basis sets, such as def2-SV(P), def2-TZVP, and def2-TZVPD, were employed. Due to computational constraints, only single-point calculations

were performed for the def2-TZVPD basis set on geometries optimized by the def2-SV(P) and def2-TZVP basis.

Table S1 in the supporting information illustrates that during gas phase adsorption of methanol, adsorption energies are independent of DFT functional and QM cluster size, significantly overestimated (too strong adsorption) with the relatively small def2-SV(P) basis set. These adsorption calculations were performed in the presence of the MM zeolite atoms represented by TraPPe-zeo force field parameters. For example, we computed with the def2-SV(P) basis set, $\Delta E_{ads,Methanol(T5)}$ = -1.87 ± 0.01 eV, $\Delta E_{ads,Methanol(T26)}$ = -1.55 ± 0.01 eV, $\Delta E_{ads,Methanol(T51)}$ = -1.44 ± 0.02 eV, and $\Delta E_{ads,Methanol(T90)}$ = -1.32 ± 0.01 eV, while the larger def2-TZVP basis set predicts 14-27% lower adsorption energies. Given that the def2-SV(P) and def2-TZVP geometries are very similar, we also computed single-point def2-TZVPD basis set calculations on def2-SV(P) and def2-TZVP optimized structures (see Table S1). This correction strategy resulted in 14-22% lower adsorption energies for methanol, highlighting that the basis set error for double zeta basis sets is unacceptably large. Figure 4 illustrates the basis set, DFT functional, and cluster size effect on the methanol adsorption energy. In addition to the basis set, we observe a large cluster size dependence in our QM/MM calculations. However, importantly, we observe that for the larger T51 and T90 clusters and with the larger def2-TZVP basis set, the methanol adsorption energy is converged with respect to the cluster size (Figure 5)[78] ($\Delta E_{ads,Methanol(T51\ or\ T90)}$ = -1.06±0.02 eV). The DFT functional effect (between ωB97-D and ωB97x-D) is minimal here (0.01-0.03 eV) for all cluster sizes and basis sets. Similar converged results were obtained for ethanol adsorption in H-MFI (see Supporting Information Figure S1 and Table S1). Specifically, (1) the energy differences introduced by the DFT functional choice

438 are small, 0.02–0.06 eV, (2) the adsorption energy converges smoothly with cluster size
439 and is converged to ~0.03 eV for the T51 cluster, and (3) basis set effects are significant
440 although they decrease with cluster size; in particular, for the T51 cluster, the energy
441 difference between def2-TZVP and def2-TZVPD basis shrinks to 0.02 eV. Thus, we
442 conclude that for methanol and ethanol adsorption energies, converged results can be
443 obtained for the T51 with the ωB97x-D/def2-TZVP level of theory.

444 *4.2 QM/MM Charge/Lennard Jones Parameter Validation*

445 During the QM/MM simulations, atoms around the QM zeolite clusters were kept
446 frozen in their crystallographic positions. For the MM atoms, it is important to identify
447 accurate charge and Lennard-Jones parameters for zeolitic Si and O atoms. We have tested
448 various combinations of charge and Lennard-Jones parameters for zeolitic silicon and
449 oxygen atoms (Q_{Si}= 0.00 to 1.50, Q_O= -0.5Q_{Si}). For zeolite silicon and oxygen Lennard-
450 Jones parameters, we have tested several published parameters for silica[79] ($\sigma_{Si} = 3.697$ Å,
451 $\sigma_O = 3.091$ Å, $\varepsilon_{Si} = 0.389$ kJ/mol and $\varepsilon_O = 0.226$ kJ/mol) and silicalite (TraPPe-zeo)[52-
452 53] ($\sigma_{Si} = 2.30$ Å, $\sigma_O = 3.30$ Å, $\varepsilon_{Si} = 0.183$ kJ/mol and $\varepsilon_O = 0.441$ kJ/mol). Both sets
453 should be compatible with the OPLS-AA[54] force field parameters for methanol and ethanol
454 (see Table S2). To identify appropriate charge parameters, we computed methanol and
455 ethanol adsorption energies considering QM cluster atoms surrounded by an uncharged
456 MM region (parameter set 1: Q_{Si} = 0.00 and Q_O = 0.00), an intermediately-charged MM
457 region (parameter set 2: Q_{Si} = 0.70 e and Q_O = -0.35 e), and a significantly-charged MM
458 region (parameter set 3: Q_{Si} = 1.50 e and Q_O = -0.75 e).

459 Figure 5 illustrates the methanol adsorption energy for the different charge models
460 for various periodic electrostatically embedded zeolite cluster models ranging from T5 to

T90. Figure S2 in the supporting information illustrates corresponding values for ethanol. We observe that the Columbic interactions are significant only for the small clusters T5 and T26. For the T51 or T90 clusters, the adsorbate is sufficiently far away from the MM zeolite atoms that the charge model has no impact on the gas phase adsorption energy. Given the sensitivity of the QM/MM adsorption energies on the Si and O charges as well as LJ parameters, we focused here on limiting their influence by selecting appropriately large cluster sizes. In the following, we continued with parameter set 3 (aligned with TraPPe-zeo force field)[48] with at least T51 clusters. We highlight that Siepmann et al. have shown that their TraPPe-zeo force field potential accurately predicts adsorption and diffusion of alcohols for a wide range of pressures and temperatures. In section 4.4, we will show that this charge parameter set also predicts a meaningful TIP4P water adsorption isotherm in H-MFI zeolite at 300 K.[48]

4.3 QM/QM Approach

Next, we continue our model validation by computing the methanol and ethanol enthalpy of adsorption at the Brønsted acidic sites of H-MFI and compare our results to both experimental results and high-level QM/QM results that do not require force field parameters. For the periodic QM/QM calculations, we used for the high-level cluster calculations ωB97x-D/def2-TZVP and subsequently corrected the energies for the cluster size effect with full periodic and cluster DFT calculations at the PBE-D3 level of theory. The key advantage of this approach is that there are no force fields involved. In Figure 6 and Table S4 in the Supporting Information, we observe a very similar adsorption enthalpy for methanol at 298K (-0.97 eV) for the H-MFI T51 cluster by the QM/MM and QM/QM approaches. Moreover, previous work by Hunger et al.[78] reported a similar heat of

adsorption of ΔH_{ads} = -0.88 eV for low coverages at 300 K using temperature programmed desorption (TPD). Also, for ethanol, the enthalpy of adsorption from force field and periodic simulation is ΔH_{ads}= -1.10 eV. This value is again in reasonably close agreement with the experimental value of ΔH_{ads} = -0.93 eV reported by Alexopoulos et al. from calorimetric tests conducted at 313K (supporting information figure S3).[80] This consistency extends to ab initio studies by Piccini et al. who reported a ΔH_{ads} of -1.08 eV at 300 K.[64]

The slight difference between theory and experiment can be understood from the simulations being performed at low Al/Si ratio at the T12 site (1 Al per unit cell), whereas the experiments having been performed on structures with high Al/Si ratio (≈ 6) and adsorption occurring on Al sites located at various T-sites. Furthermore, the experimental results are often being only available for adsorption within zeolites when adsorption sites are more densely populated with lateral interactions between the adsorbed species.[64,80] For the T5 and T26 clusters, major differences between simulated enthalpic values (ΔH_{ads}) and experimental data has been observed due to alcohol oxygen's binding capacity with zeolitic hydrogen (Al12-O20(H)-Si3). The PBE-D3 cluster size correction factor in the periodic QM/QM approaches displays a significant impact of 0.10 eV for the small T5 and/or T26 clusters. However, its effect becomes minimal for larger clusters such as T51 or T90.

Finally, we would like to highlight the QM/MM force field technique for liquid-phase modeling, allowing us to simulate the effect of classical water molecules within zeolites on the energetics of other adsorbates. Given the results described above we selected a T51 cluster for the liquid phase simulations. We expect simulations to be converged with cluster size while still being affordable. We note that the computational

cost is highly influenced by the size of the clusters employed. For instance, a T51 cluster consists of 180 atoms and a T90 cluster consists of 314 atoms which is 8-15 times larger than a T5 cluster with 22 atoms. Table 1 shows computational times during methanol adsorption in H-MFI for different clusters.

4.4 Adsorption in Condensed/Liquid Phase Environments

In this investigation of solvent (water) effects on methanol and ethanol adsorption in H-MFI zeolite, our first task was to ensure that a condensed phase environment of the solvent is formed inside the zeolite pore structure during the simulations. This involved performing grand canonical Monte Carlo (GCMC) simulations at a temperature of 298 K and different chemical potentials. Specifically, each GCMC simulation involved 100 million Monte Carlo (MC) steps. After about 20 million equilibration steps the number of water molecules in the zeolite framework stayed approximation constant. Thus, we used the last 50 million steps for sampling of the configuration space and free energy computations. As expected, variations in chemical water potential have a direct influence on the phase transition behavior of the TIP4P water model within the bulk and pore water phase. Figure S4 in the Supporting Information illustrates a phase change of bulk water (gas to liquid), when the chemical potential increased from -45 kJ/mol to -44 kJ/mol. Similarly, inside the zeolite pore structure, pore condensation can be observed when the water chemical potential increases from -48 kJ/mol to -47 kJ/mol (Figure S4). The lower critical chemical potential at which pore condensation can be observed (relative to condensation in the bulk) agrees with the literature and can be explained by the attractive interactions of the pore wall with the water molecules.[81, 82] We conclude that at bulk phase transition water chemical potentials of μ_{bulk}= -44 kJ/mol, the H-MFI zeolite pore structure

530 is filled with water and small changes in water chemical potential have only a small effect
531 on the number of water molecules in the zeolite structure.

532 Next, we need to assign charges to all atoms, including the QM atoms, in our
533 simulation system to perform the necessary GCMC simulations for the FEP calculations
534 with our electrostatically embedded hybrid QM/MM Hamiltonian. Here, we used scaled
535 NPA charges and the fixed charge approximation for the zeolite-adsorbate T51 cluster
536 atoms. This strategy aimed to achieve comparable charges for the Si and O atoms of the
537 zeolite framework in both the QM and MM subsystems, i.e., Q_{Si} = +1.50 e and $Q_O \approx$ -0.75
538 e. By scaling all QM atom charges to relaxed Si charges of 1.50 e, we ensured a similar
539 water adsorption behavior throughout the simulation system while maintaining
540 electrostatic neutrality for the cluster, including its terminal hydrogen atoms, and the
541 overall system (Table 2). Non-scaled NPA charges and DDEC6[83] charges (Table S3 of the
542 Supporting Information) led to significant deviations between the charges on the MM and
543 QM subsystem atoms, which is undesirable as it will also lead to an uneven water
544 adsorption behavior.

545 We note that the zeolite acid proton can be mobile in the presence of condensed
546 water forming hydronium ions (H_3O^+) inside the H-MFI zeolite pore structure. In
547 particular, this has been observed for systems with relatively low Si/Al ratio (6, 15, 23 and
548 40).[84, 85] Given that this study deals with a high Si/Al ratio of the zeolite (>95), we expect
549 the proton to reside close to the aluminum site and to a first approximation we are
550 neglecting here any complications that originate from the proton delocalizing into the
551 liquid water phase. In future studies, we will investigate the role proton delocalization on
552 the adsorption free energy of alcohols.

As described in Section 3.3, the aqueous-phase effect on the free energy of adsorption is estimated using our QM/MM-FEP scheme. Figures 7(A) and 7(B) show the free-energy profile of the solvation effects on the desorption of methanol and ethanol from H-MFI. The profiles are comprised of five sub-sections: $1_{opt,0}$-to-1, 1-to-2 (Electrostatic interaction removal), 2-to-3 (Electrostatic Embedding), 3-to-4 (Lennard-Jones potential removal), and 4-to-4_{opt} (zeolite QM/MM-FEP only), whose individual values are listed in Table 3. Overall, methanol and ethanol are destabilized (Table 4) in H-MFI by the presence of condensed water ($\Delta\Delta G^{liq\rightarrow gas}_{methanol,QM/MM-FEP} = +0.44$ eV and $\Delta\Delta G^{liq\rightarrow gas}_{ethanol,QM/MM-FEP} = +0.54$ eV), somewhat similar to what we observed for metal surfaces, although the solvent effect is lower in zeolites, probably because of a reduced water density in a zeolite pore relative to a metal surface.[73,74] Nevertheless, similar to alcohol absorption in water,[86] we compute overall a favorable methanol and ethanol adsorption in aqueous H-MFI, see Table 4 ($\Delta G^{gas\rightarrow liq}_{ads}$).

For methanol and ethanol adsorption in H-MFI zeolite at 298 K, free energy changes for the shift in zeolite structure from those in an empty vapor phase optimized system to those of a methanol and ethanol adsorbed system, $1_{opt,0} \rightarrow 1_{opt}$, are 0.21 and 0.23 eV, respectively. The QM atom coordinate transition from liquid phase optimized coordinates to vapor phase optimized coordinates (1_{opt}-to-1) in the condensed phase subsystem result in only a small free energy change ($\Delta\Delta G_{1_{opt}-to-1,methanol} = 0.01$ eV and $\Delta\Delta G_{1_{opt}-to-1,ethanol} = 0.04$ eV), indicating a small change in adsorbate structure due to the presence of water.

Next, electrostatic interactions removal, step 1-to-2, between the TIP4P water molecules and the adsorbates slightly destabilized the adsorbed species $\left(\Delta\Delta G^{liq\rightarrow gas}_{\text{Electrostatic Removal, Methanol}} = -0.04 \text{ eV} \text{ and } \Delta\Delta G^{liq\rightarrow gas}_{\text{Electrostatic Removal, Ethanol}} = -0.05 \text{ eV}\right)$. Although the impact is small, it highlights how net repulsive, electrostatic forces can be present, due to a high density of molecules in the pore structure. We observed that during the electrostatic interaction removal step the net charge of the adsorbates (methanol or ethanol) mostly transferred to the H-MFI zeolite's Brønsted hydrogen/proton $\left(\Delta Q_{\text{Hydrogen,Proton,1-to-2}} = +0.03\right)$ and nearby oxygen atom (Al_{12}-O_{20}(H)-Si_3) attached to the Brønsted acidic site $\left(\Delta Q_{\text{Oxygen,1-to-2}} = +0.03\right)$.

From state 2-to-3, the non-classical contributions of water molecules changing the electronic structure of the quantum system transition from those of a zeolite-adsorbate system to those without adsorbate, i.e., this energy difference constitutes the main difference between electrostatic and mechanical embedding of the QM/MM system. Here, we observed that the water molecules destabilize the adsorption of methanol and ethanol inside the zeolite during electronic structural modifications, where the adsorption energy varies with size of the adsorbate and its interaction with Brønsted acidic sites. Specifically, we compute $\Delta\Delta G^{liq\rightarrow gas}_{\text{2-to-3, Methanol}} = -0.04 \text{ eV}$ and $\Delta\Delta G^{liq\rightarrow gas}_{\text{2-to-3, Ethanol}} = -0.05 \text{ eV}$, a small but significant effect of electrostatic embedding.

When the Lennard-Jones interactions between the water molecules and the adsorbates are removed in the QM/MM-FEP scheme, the solvent cavity inside the zeolite for methanol and ethanol shrinks, a significant exergonic process

$\left(\Delta\Delta G^{liq\rightarrow gas}_{vdW\ Removal,\ Methanol} = -0.42\ eV \text{ and } \Delta\Delta G^{liq\rightarrow gas}_{vdW\ Removal,\ Ethanol} = -0.55\ eV\right)$ that scales with the size of the adsorbate.

Finally, during 4-to-4_{opt} the zeolite atom coordinates in liquid water change to the optimized coordinates of a free zeolite site. This aspect holds similar importance to the energy difference between $1_{opt,0}$-to-1_{opt}. However, unlike $1_{opt,0}$-to-1_{opt} where a simple energy computation can predict the energy difference, QM/MM-FEP calculations are necessary to compute this energy difference $\left(\Delta\Delta G^{liq\rightarrow gas}_{4-to-4_{opt},\ Methanol} = -0.16\ eV \text{ and } \Delta\Delta G^{liq\rightarrow gas}_{4-to-4_{opt},\ Ethanol} = -0.15\ eV\right)$.

5. CONCLUSION

We developed a QM/MM FEP method to investigate the adsorption behavior of methanol and ethanol inside H-MFI zeolite in the presence of a mean field of condensed water described by the TIP4P water model. Our methodology, which we call eSZS, can easily be generalized to any porous, insulating system. Initially, gas phase hybrid QM/MM simulations were performed to determine meaningful zeolitic QM cluster sizes, DFT functionals, basis sets, and charge and Lennard Jones parameters. Consistent adsorption energies for methanol and ethanol were obtained at 298 K ($\Delta H_{ads,\ methanol}$= -0.97 eV and $\Delta H_{ads,\ ethanol}$= -1.10 eV) using an electrostatically embedded T51 QM cluster with ωB97x-D/def2-TZVP level of theory and TraPPe-zeo force field.

Next, we modeled the absolute condensed water phase effect on the methanol and ethanol adsorption free energy. Highlights of our method are the sampling of water with grand-canonical Monte Carlo (μVT) simulations to compute the mean electrostatic effect of water on the DFT calculations, the ability to optimize adsorbates in the presence of the condensed phase, and the development of a system Hamiltonian and thermodynamic cycle

618 that permits rapid FEP calculations for the absolute solvent effect by removal of the
619 interactions between water and the adsorbate. As long as the interactions between the
620 solvent and the adsorbate can be described by classical pair potentials, and adsorption is
621 primarily localized, our hybrid QM/MM method is highly efficient and at most two orders
622 of magnitude more expensive (computationally) than regular gas phase calculations.

623 Finally, we computed aqueous solvation free energies for methanol and ethanol in
624 H-MFI (with high Si/Al ratio > 95) at 298 K of $\Delta\Delta G^{gas\rightarrow liq}_{methanol,\frac{QM}{MM}-FEP} = 0.44 \pm$
625 0.006 eV and $\Delta\Delta G^{gas\rightarrow liq}_{ethanol,\frac{QM}{MM}-FEP} = 0.541 \pm 0.005$ eV indicating a destabilization in the
626 presence of condensed water due to the need to form a water free cavity. Future applications
627 of our methodology include studying condensed phase effects on adsorption of
628 contaminants of emerging concern in wastewater and hydrocracking of hydrocarbons in
629 zeolites in the presence of water. While for many adsorbates the localized approximation
630 might not be excellent, we expect it to be very good for transition states and many strongly
631 binding species.

632 **6. SUPPORTING INFORMATION**

633 Gas phase adsorption energies with different basis sets and functionals; Lennard-
634 Jones parameters; charge analysis; comparison of NPA, DDEC6, and scaled NPA charge
635 model; QM/QM adsorption energies for various cluster sizes; ethanol adsorption energy
636 with different Si/O charges; QM/MM and QM/MM model comparison for ethanol
637 adsorption enthalpy; bulk TIP4P water chemical potential.

638 **7. ACKNOWLEDGMENTS**

The Department of Energy, Office of Basic Energy Science, Catalysis Science program supported this research with award number DESC0007167. Additionally, the National Science Foundation (NSF) funded the initial studies of the presented research under grant number OIA-1632824. Partial funding for this project also came from the South Carolina State Center for Strategic Approaches to Electricity Generation (SAGE). The research team would like to express gratitude for the computational resources provided by various entities. The National Energy Research Scientific Computing Center (NERSC), supported by the Office of Science of the U.S. Department of Energy (DOE), the Extreme Science and Engineering Discovery Environment (XSEDE) from the Texas Advanced Computing Center (TACC) at the University of Texas at Austin, under grant number TG-CTS090100, the Environmental Molecular Sciences Laboratory (EMSL) under the Pacific Northwest National Laboratory (PNNL) and the High Performance Computing (HPC) Group at the University of South Carolina are greatly acknowledged and contributed essential computational resources that enabled the research to progress.

8. TABLES AND FIGURES

Table 1: Approximate computational cost for an energy calculation of a periodic electrostatically embedded QM cluster calculation with adsorbed methanol for different clusters and basis sets relative to a cluster containing five Si and Al atoms (T5).

Functional/Basis Sets	T5	T26	T51	T90
ωB97x-D/def2-TZVP	1x	58x	510x	1300x
ωB97x-D/def2-TZVPD	12x	280x	850x	N/A

Table 2: Charge model selection for liquid phase modeling inside H-MFI. During this charge analysis, we used different charge parameters for the MM atoms (Q_{Si} = +0.0 to +1.50, Q_O = 0.0 to −0.75). First, we performed a natural population analysis (non-scaled NPA) in the PEECM calculation to obtain charges of the T51 cluster atoms. For these charges, we did not observe any significant difference between the bulk water vapor-liquid and pore vapor-liquid phase transitioning chemical potential. More importantly, the water distribution inside the zeolite was very uneven in the QM cluster and MM area of the simulation system. The same occurred when we used the DDEC6 method[83] to determine the charges. Finally, we used scaled NPA charges, where we scaled the average silicon charges to those of the TraPPe-zeo force field parameters for MM atoms - silicon (Q_{Si} = +1.50). In these calculations, we observed water pore condensation ($\mu_{Pore\ water} < \mu_{bulk\ water}$) and an even distribution of water within zeolite supercell and around the T51 QM cluster embedded inside the zeolite. See Table S3 in the SI with more details on the charges used in the Scaled NPA simulation system.

	QM Atom Charges (Averaged)				Bulk Phase Transitioning chemical potential (μ_{bulk} kJ/mol)	Pore Phase Transitioning chemical potential (μ_{pore} kJ/mol)
Charge Analysis Method	Si (Relaxed in the T51 cluster)	Si (Fixed in the T51 cluster)	O (Relaxed in T51 cluster)	H (Terminal)		
Non-Scaled NPA	2.56	2.16	−1.27	−0.35	−44.0	−44.0
DDEC6	1.92	1.92	−0.96	N/A		−44.0
Scaled NPA	1.50	1.50	−0.75	−0.21		−47.0

Table 3: Aqueous solvent effect (TIP4P water) on the free energy (in eV) of methanol and ethanol desorption in H-MFI at 298 K (T12 Bronsted acid site). All numbers include a 95% confidence interval based on water samples acquired from numerous independent simulations.

Adsorbate	**$1_{opt,0}$-to-1_{opt}** (Vapor phase coordinate change)	**1_{opt}-to-1** (Adsorbate optimization in liquid)	**1-to-2** (Electrostatic interaction removal)	**2-to-3** (Electrostatic Embedding)	**3-to-4** (Lennard-Jones potential removal)	**4-to-4_{opt}** (QM/MM-FEP Zeolite Only)
Methanol	0.21	0.01±0.001	-0.04±0.001	-0.04±0.002	-0.42±0.001	-0.16±0.001
Ethanol	0.23	0.04±0.002	-0.05±0.001	-0.05±0.001	-0.55±0.001	-0.15±0.001

Table 4: Aqueous solvent effect on the free energy of methanol and ethanol adsorption at the T12 Bronsted acid site in H-MFI at 298K. The reference state is methanol and ethanol at a fugacity of 1 bar.

Adsorbate	ΔG_{ads}^{gas} (eV)	$\Delta\Delta G_{ads,QM/MM-FEP}^{gas\rightarrow liq}$ (eV)	$\Delta G_{ads}^{gas\rightarrow liq}$(eV)
Methanol	-0.61	0.44 ± 0.006	-0.17 ± 0.006
Ethanol	-0.75	0.54 ± 0.005	-0.21 ± 0.005

1

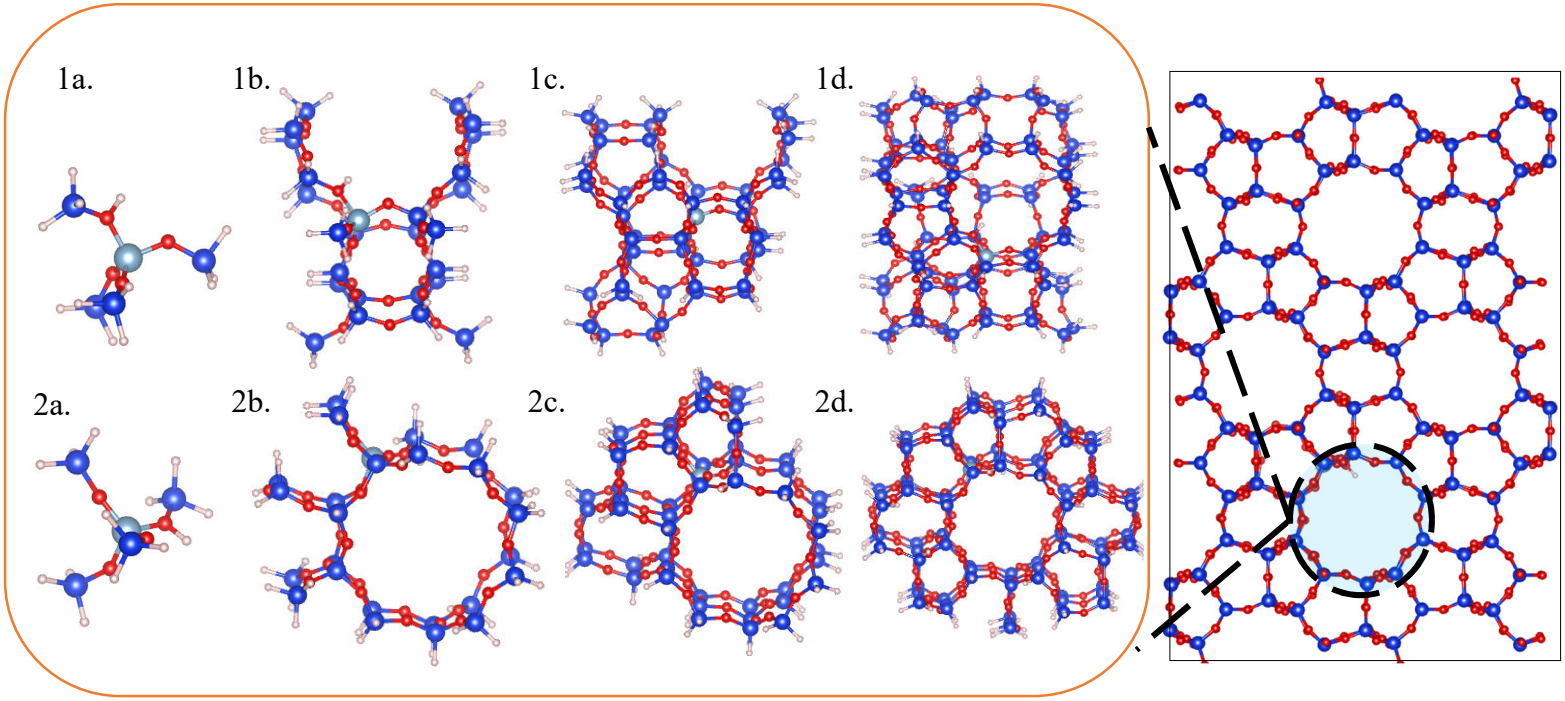

Figure 1: Four different (a) T5 (b) T26 (c) T51 (d) T90 cluster models have been taken from a periodic H-MFI zeolite supercell. Top set of models (1a – 1d) show the view through the sinusoidal channel on the T12 site in MFI and lower set of models (2a – 2d) show the view through the straight channel. Color codes: Silicon (Deep Blue), Aluminum (Sky Blue), Hydrogen (White) and Oxygen (Red).

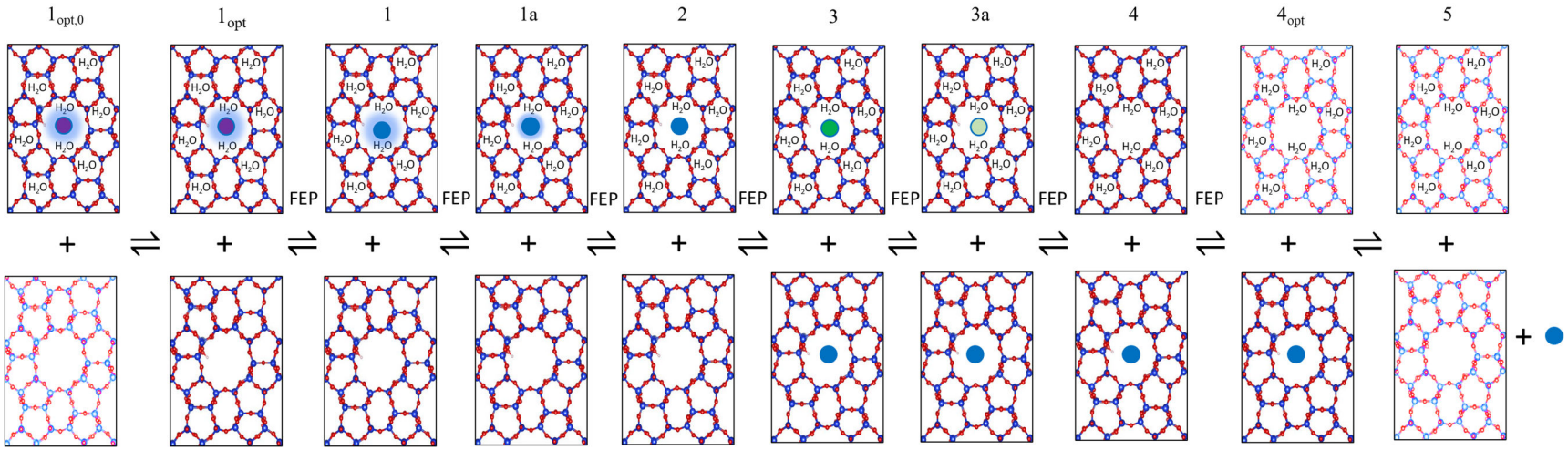

Figure 2. Thermodynamic cycle for computing the aqueous solvent effect on the adsorption free energy of an adsorbate at an active site in a porous medium such as H-MFI zeolite in the presence of liquid water. The adsorbate is illustrated as ● in a gas phase environment and as ● in an aqueous environment, i.e., adsorption in the presence of liquid water is illustrated as, ● (g) + *(l) ↔ ● *(l), where * symbolizes the active site in H-MFI, gas phase adsorption is illustrated as, ● (g) + *(g) ↔ ●*(g)), and the solvent effect on adsorption is described as: *(l) + ● *(g) ↔ ● *(l) + *(g). Between states $1_{opt,0}$ and 1_{opt}, the coordinates of the zeolite structure shift from those in the vapor phase optimized system to those of a system optimized with adsorbate. The liquid phase system remains unchanged. Between state 1_{opt} to 1, the coordinates of the adsorbate atoms described by DFT in the liquid phase system transition from liquid to vapor phase optimized coordinates. There is no change in the vapor phase system. In the liquid phase system, the (classical) electrostatic interaction between the water solvent and the adsorbate is gradually removed between states 1 and 2, where no change of quantum atom coordinates happens. Intermediate states, such as state 1a, are considered "non-physical" in QM/MM-FEP calculations. The "non-classical" contributions of water molecules changing the quantum system's electronic structure transition from a zeolite-adsorbate system to one without adsorbate is described from state 2 to 3, i.e., this energy difference is the main difference between electrostatic and mechanical embedding of the QM/MM system. The adsorbate is only present in the classical (Monte Carlo) simulation and not in the quantum system, as indicated by ●. Between states 3 and 4, the van der Waals interactions between the solvent water molecules and the adsorbate are gradually removed. Quantum atom coordinates do not change. State 3a, for example, is a "non-physical" intermediate state. The zeolite

atom coordinates in liquid change from state 4 to state 4_{opt}, where they become the optimized coordinates of a free site in the porous medium. In the vapor phase system, nothing changes. Between states 4_{opt} and 5, gas-phase desorption is described. The solvent influence on adsorbate stability in solvent is represented by the (free) energy difference between states 4_{opt} and $1_{opt,0}$.

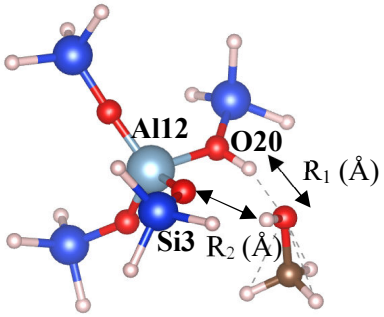

T5: R_1 = 1.28 Å and R_2 = 2.11 Å

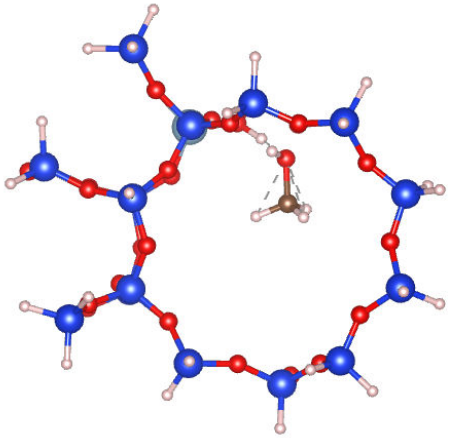

T26: R_1 = 1.36 Å and R_2 = 2.17 Å

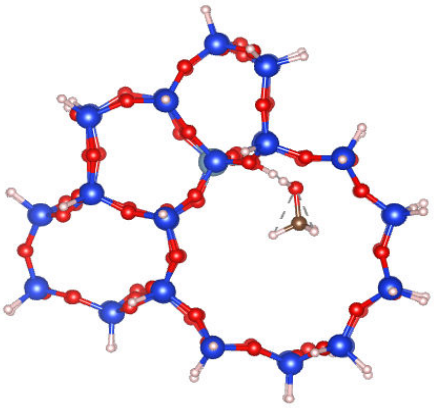

T51: R_1 = 1.46 Å and R_2 = 2.18 Å

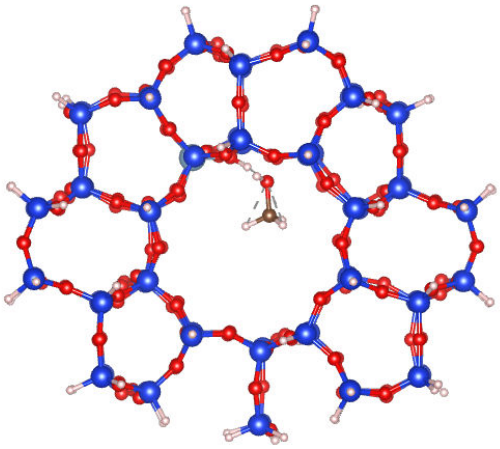

T90: R_1 = 1.48 Å and R_2 = 2.39 Å

Figure 3: Methanol adsorption in different H-MFI zeolite clusters T5, T26, T51, and T90. R_1 is the distance between the zeolitic hydrogen [Al_{12}-O_{20}(H)-Si_3] and the oxygen of adsorbed methanol. R_2 is the distance between the OH hydrogen of adsorbed methanol and the nearest zeolitic oxygen atom. Color code – blue is silicon, red is oxygen, white is hydrogen, silver blue is aluminum and dark grey is carbon.

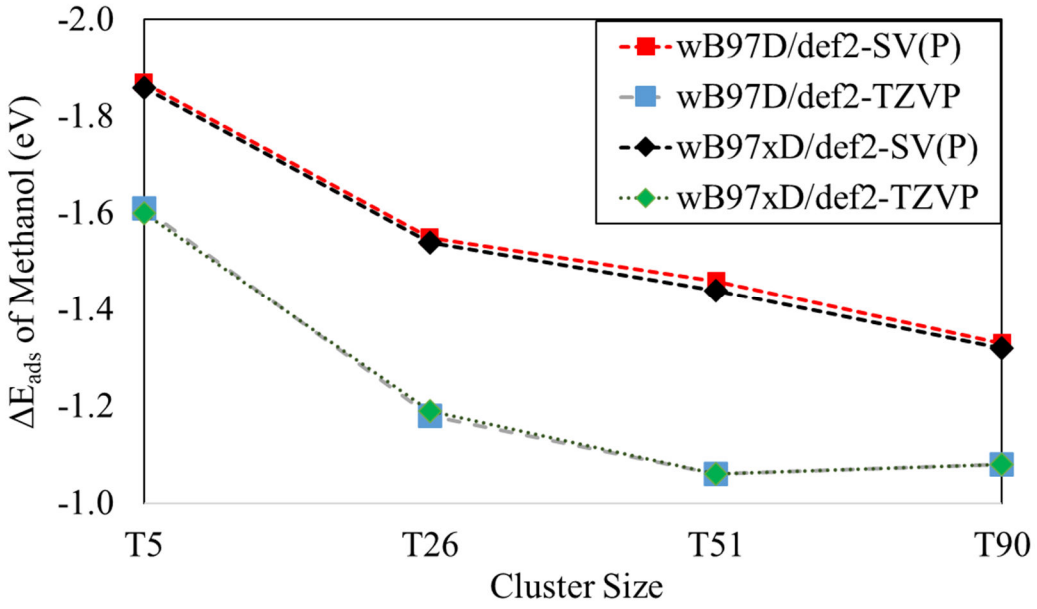

Figure 4: Adsorption energy of methanol in H-MFI. Comparison of predicted adsorption energy using the ωB97-D/def2-SV(P), ωB97-D/def2-TZVP, ωB97x-D/def2-SV(P), and ωB97x-D/def2-TZVP methods in our periodic embedded cluster models of increasing size (T5, T26, T51, T90).

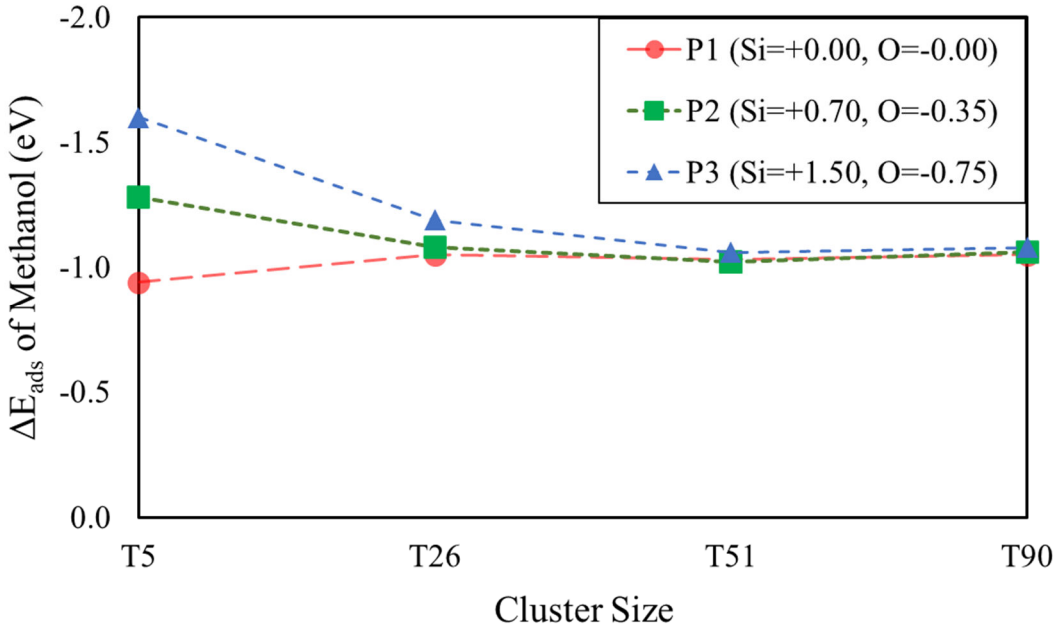

Figure 5: Adsorption energy of methanol in H-MFI (ωB97x-D/def2-TZVP). Comparison of different charge parameters (three sets) with TraPPe-zeo Lennard-Jones (σ, ε) values for zeolite Si and O.

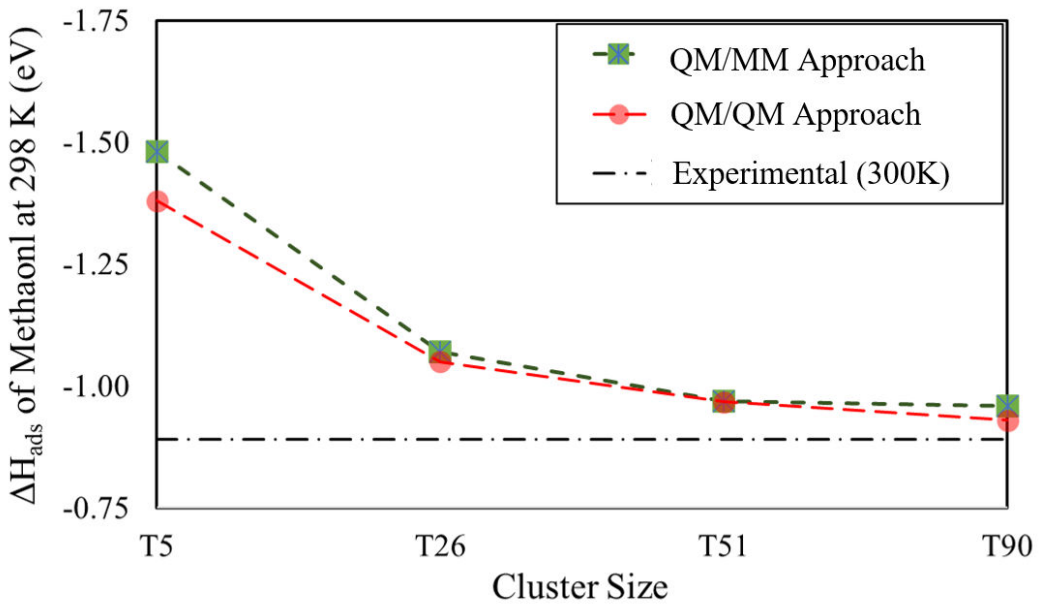

Figure 6: Comparison of QM/MM approach and QM/QM approach for calculating the gas phase adsorption enthalpy (ΔH_{ads}) of methanol in H-MFI zeolite at 298K. Experimental results are obtained from Hunger et al.[78]

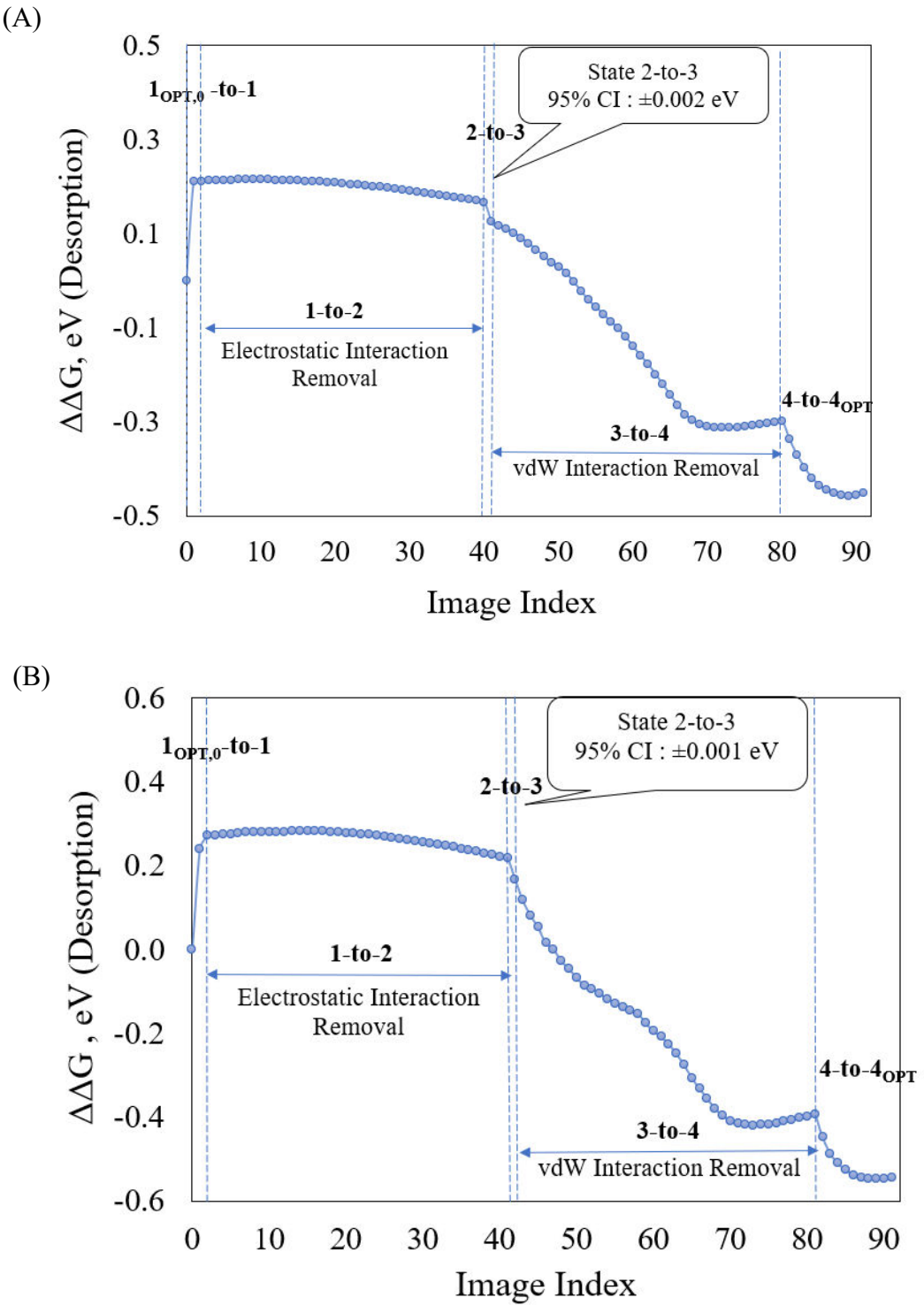

Figure 7: Free-energy (potential of mean force) profiles for aqueous-phase effects on the desorption $\left(\Delta\Delta G^{liq\rightarrow gas}_{Desorption} = -\Delta\Delta G^{gas\rightarrow liq}_{Adsorption}\right)$ of (A) methanol and (B) ethanol from H-MFI zeolite.

9. BIBLIOGRAPHY

1. Ruthven, D. M. *Principles of Adsorption and Adsorption Processes*; John Wiley & Sons, 1984.

2. Haag, W. O. Catalysis by Zeolites – Science and Technology; Elsevier, 1994; Vol. 84, pp 1375–1394.

3. Mellmer, M. A.; Sener, C.; Gallo, J. M. R.; Luterbacher, J. S.; Alonso, D. M.; Dumesic, J. A. Solvent Effects in Acid-Catalyzed Biomass Conversion Reactions. *Angewandte Chemie International Edition* **2014**, *53* (44), 11872–11875.

4. Haw, J. F.; Xu, T.; Nicholas, J. B.; Goguen, P. W. Solvent-Assisted Proton Transfer in Catalysis by Zeolite Solid Acids. *Nature* **1997**, *389* (6653), 832–835.

5. Hölderich, W.; Hesse, M.; Näumann, F. Zeolites: Catalysts for Organic Syntheses. *Angewandte Chemie International Edition in English* **1988**, *27* (2), 226–246.

6. Corma, A. Inorganic Solid Acids and Their Use in Acid-Catalyzed Hydrocarbon Reactions. *Chem. Rev.* **1995**, *95* (3), 559–614.

7. Sen, S. E.; Smith, S. M.; Sullivan, K. A. Organic Transformations Using Zeolites and Zeotype Materials. *Tetrahedron* **1999**, *55* (44), 12657–12698.

8. Loera, S.; Lima, E.; Pfeiffer, H.; Lara, V. Synthesis of Aluminosilicates under High Pressure and Using Sulfur as Directing Agent. *Open Chemistry* **2012**, *10* (1), 105–112.

9. Guisnet, M., Gilson, J. P., Hutchings, G. J. Zeolites for Cleaner Technologies. *J. Am. Chem. Soc.* **2003**, *125* (22), 6839–6839.

10. Valyon, J.; Onyestyák, G.; Rees, L. V. C. Study of the Dynamics of NH_3 Adsorption in ZSM-5 Zeolites and the Acidity of the Sorption Sites Using the Frequency-Response Technique. *J. Phys. Chem. B* **1998**, *102* (45), 8994–9001.

11. Farneth, W. E.; Gorte, R. J. Methods for Characterizing Zeolite Acidity. *Chem. Rev.* **1995**, *95* (3), 615–635.

12. Zecchina, A.; Geobaldo, F.; Spoto, G.; Bordiga, S.; Ricchiardi, G.; Buzzoni, R.; Petrini, G. FTIR Investigation of the Formation of Neutral and Ionic Hydrogen-Bonded Complexes by Interaction of H-ZSM-5 and H-Mordenite with CH_3CN and H_2O: Comparison with the H-NAFION Superacidic System. *J. Phys. Chem.* **1996**, *100* (41), 16584–16599.

13. Lónyi, F.; Valyon, J. A TPD and IR Study of the Surface Species Formed from Ammonia on Zeolite H-ZSM-5, H-Mordenite and H-Beta. *Thermochimica Acta* **2001**, *373* (1), 53–57.

14. Lónyi, F.; Valyon, J. On the Interpretation of the NH3-TPD Patterns of H-ZSM-5 and H-Mordenite. *Microporous and Mesoporous Materials* **2001**, *47* (2), 293–301.

15. Boréave, A.; Auroux, A.; Guimon, C. Nature and Strength of Acid Sites in HY Zeolites: A Multitechnical Approach. *Microporous Materials* **1997**, *11* (5), 275–291.

16. Kao, H.-M.; Grey, C. P. Probing the Brønsted and Lewis Acidity of Zeolite HY: A 1H/27Al and 15N/27Al TRAPDOR NMR Study of Monomethylamine Adsorbed on HY. *J. Phys. Chem.* **1996**, *100* (12), 5105–5117.

17. Zheng, A.; Han, B.; Li, B.; Liu, S.-B.; Deng, F. Enhancement of Brønsted Acidity in Zeolitic Catalysts Due to an Intermolecular Solvent Effect in Confined Micropores. *Chem. Commun.* **2012**, *48* (55), 6936–6938.

18. Jacobs, W. P. J. H.; de Haan, J. W.; van de Ven, L. J. M.; van Santen, R. A. Interaction of Ammonia with Brønsted Acid Sites in Different Cages of Zeolite Y as Studied by Proton MAS NMR. *J. Phys. Chem.* **1993**, *97* (40), 10394–10402.

19. Katada, N.; Igi, H.; Kim, J.-H. Determination of the Acidic Properties of Zeolite by Theoretical Analysis of Temperature-Programmed Desorption of Ammonia Based on Adsorption Equilibrium. *J. Phys. Chem. B* **1997**, *101* (31), 5969–5977.

20. Brueva, T. R.; Mishin, I. V.; Kapustin, G. I. Distribution of Acid-Site Strengths in Hydrogen Zeolites and Relationship between Acidity and Catalytic Activity. *Thermochimica Acta* **2001**, *379* (1), 15–23.

21. Catlow, C. R. A.; Bell, R. G.; Gale, J. D.; Lewis, D. W. Modelling of Structure and Reactivity in Zeolites. In *Studies in Surface Science and Catalysis*; Bonneviot, L., Kaliaguine, S., Eds.; Zeolites: A Refined Tool for Designing Catalytic Sites; Elsevier, 1995; Vol. 97, pp 87–100.

22. *Computer Modelling of Microporous Materials*; Catlow, C. R. A., Santen, van, R. A., Smit, B., Series Eds.; Academic Press Inc.: Amsterdam, 2004.

23. Bai, P.; Neurock, M.; Siepmann, J. I. First-Principles Grand-Canonical Simulations of Water Adsorption in Proton-Exchanged Zeolites. *J. Phys. Chem. C* **2021**, *125* (11), 6090–6098

24. DeJaco, R. F.; Bai, P.; Tsapatsis, M.; Siepmann, J. I. Adsorptive Separation of 1-Butanol from Aqueous Solutions Using MFI- and FER-Type Zeolite Frameworks: A Monte Carlo Study. *Langmuir* **2016**, *32* (8), 2093–2101.

25. Narasimhan, L.; Boulet, P.; Kuchta, B.; Schaef, O.; Denoyel, R.; Brunet, P. Molecular Simulations of Water and Paracresol in MFI Zeolite - A Monte Carlo Study. *Langmuir* **2009**, *25* (19), 11598–11607.

26. Bellat, J.-P.; Paulin, C.; Jeffroy, M.; Boutin, A.; Paillaud, J.-L.; Patarin, J.; Di Lella, A.; Fuchs, A. Unusual Hysteresis Loop in the Adsorption−Desorption of Water in NaY Zeolite at Very Low Pressure. *J. Phys. Chem. C* **2009**, *113* (19), 8287–8295.

27. Abrioux, C.; Coasne, B.; Maurin, G.; Henn, F.; Boutin, A.; Di Lella, A.; Nieto-Draghi, C.; Fuchs, A. H. A Molecular Simulation Study of the Distribution of Cation in Zeolites. *Adsorption* **2008**, *14* (4), 743–754.

28. Guo, X.; Huang, S.; Teng, J.; Xie, Z. Study on Adsorption of Water on NanZSM-5 Type Zeolite by Molecular Simulation. *Acta Physico-Chimica Sinica* **2006**, *22* (3), 270–274.

29. Özgür Yazaydın, A.; Thompson, R. W. Molecular Simulation of Water Adsorption in Silicalite: Effect of Silanol Groups and Different Cations. *Microporous and Mesoporous Materials* **2009**, *123* (1), 169–176.

30. Ramachandran, C. E.; Chempath, S.; Broadbelt, L. J.; Snurr, R. Q. Water Adsorption in Hydrophobic Nanopores: Monte Carlo Simulations of Water in Silicalite. *Microporous and Mesoporous Materials* **2006**, *90* (1), 293–298

31. Grimme, S.; Antony, J.; Ehrlich, S.; Krieg, H. A Consistent and Accurate Ab Initio Parametrization of Density Functional Dispersion Correction (DFT-D) for the 94 Elements H-Pu. *J. Chem. Phys.* **2010**, *132* (15), 154104.

32. Lee, K.; Murray, É. D.; Kong, L.; Lundqvist, B. I.; Langreth, D. C. Higher-Accuracy van Der Waals Density Functional. *Phys. Rev. B* **2010**, *82* (8), 081101.

33. Blaszkowski, S. R.; Nascimento, M. A. C.; van Santen, R. A. Activation of C−H and C−C Bonds by an Acidic Zeolite: A Density Functional Study. *J. Phys. Chem.* **1996**, *100* (9), 3463–3472.

34. Boronat, M.; Viruela, P. M.; Corma, A. Reaction Intermediates in Acid Catalysis by Zeolites: Prediction of the Relative Tendency To Form Alkoxides or Carbocations as a Function of Hydrocarbon Nature and Active Site Structure. *J. Am. Chem. Soc.* **2004**, *126* (10), 3300–3309.

35. Rozanska, X.; Demuth, Th.; Hutschka, F.; Hafner, J.; van Santen, R. A. A Periodic Structure Density Functional Theory Study of Propylene Chemisorption in Acidic Chabazite: Effect of Zeolite Structure Relaxation. *J. Phys. Chem. B* **2002**, *106* (12), 3248–3254.

36. Lo, C.; Trout, B. L. Density-Functional Theory Characterization of Acid Sites in Chabazite. *Journal of Catalysis* **2004**, *227* (1), 77–89.

37. Hafner, J.; Wolverton, C.; Ceder, G. Toward Computational Materials Design: The Impact of Density Functional Theory on Materials Research. *MRS Bull.* **2006**, *31* (9), 659–668.

38. Hansen, N.; Kerber, T.; Sauer, J.; Bell, A. T.; Keil, F. J. Quantum Chemical Modeling of Benzene Ethylation over H-ZSM-5 Approaching Chemical Accuracy: A Hybrid MP2:DFT Study. *J. Am. Chem. Soc.* **2010**, *132* (33), 11525–11538.

39. Tuma, C.; Kerber, T.; Sauer, J. The Tert-Butyl Cation in H-Zeolites: Deprotonation to Isobutene and Conversion into Surface Alkoxides. *Angewandte Chemie International Edition* **2010**, *49* (27), 4678–4680.

40. Zhao, Y.; Truhlar, D. G. Benchmark Data for Interactions in Zeolite Model Complexes and Their Use for Assessment and Validation of Electronic Structure Methods. *J. Phys. Chem. C* **2008**, *112* (17), 6860–6868.

41. Zhao, Y.; Truhlar, D. G. A Density Functional That Accounts for Medium-Range Correlation Energies in Organic Chemistry. *Org. Lett.* **2006**, *8* (25), 5753–5755..

42. Zhao, Y.; Truhlar, D. G. Construction of a Generalized Gradient Approximation by Restoring the Density-Gradient Expansion and Enforcing a Tight Lieb–Oxford Bound. *J. Chem. Phys.* **2008**, *128* (18), 184109.

43. Chai, J.-D.; Head-Gordon, M. Long-Range Corrected Hybrid Density Functionals with Damped Atom–Atom Dispersion Corrections. *Physical Chemistry Chemical Physics* **2008**, *10* (44), 6615–6620.

44. Chai, J.-D.; Head-Gordon, M. Long-Range Corrected Double-Hybrid Density Functionals. *J. Chem. Phys.* **2009**, *131* (17), 174105.

45. Olson, D.; Kokotailo, G. T.; Lawton, S. L.; Meier, W. M. Crystal Structure and Structure-Related Properties of ZSM-5. **1981**.

46. Olson, D. H.; Khosrovani, N.; Peters, A. W.; Toby, B. H. Crystal Structure of Dehydrated CsZSM-5 (5.8Al): Evidence for Nonrandom Aluminum Distribution. *J. Phys. Chem. B* **2000**, *104* (20), 4844–4848.

47. Mentzen, B. F.; Sacerdote-peronnet, M. Prediction of Preferred Proton Locations in HMFI/Benzene Complexes by Molecular Mechanics Calculations. Comparison with Nmr, Structural and Calorimetric Results. *Materials Research Bulletin* **1994**, *29* (12), 1341–1348

48. Bai, P.; Tsapatsis, M.; Siepmann, J. I. TraPPE-Zeo: Transferable Potentials for Phase Equilibria Force Field for All-Silica Zeolites. *J. Phys. Chem. C* **2013**, *117* (46), 24375–24387.

49. Ahlrichs, R.; Bär, M.; Häser, M.; Horn, H.; Kölmel, C. Electronic Structure Calculations on Workstation Computers: The Program System Turbomole. *Chemical Physics Letters* **1989**, *162* (3), 165–169.

50. Treutler, O.; Ahlrichs, R. Efficient Molecular Numerical Integration Schemes. *J. Chem. Phys.* **1995**, *102* (1), 346–354.

51. Schwenk, C. F.; Rode, B. M. Influence of Electron Correlation Effects on the Solvation of Cu2+. *J. Am. Chem. Soc.* **2004**, *126* (40), 12786–12787.

52. Gomes, J.; Zimmerman, P. M.; Head-Gordon, M.; Bell, A. T. Accurate Prediction of Hydrocarbon Interactions with Zeolites Utilizing Improved Exchange-Correlation Functionals and QM/MM Methods: Benchmark Calculations of Adsorption Enthalpies and Application to Ethene Methylation by Methanol. J. Phys. Chem. C 2012, 116 (29), 15406–15414.

53. Zimmerman, P. M.; Head-Gordon, M.; Bell, A. T. Selection and Validation of Charge and Lennard-Jones Parameters for QM/MM Simulations of Hydrocarbon Interactions with Zeolites. J. Chem. Theory Comput. 2011, 7 (6), 1695–1703.

54. Jorgensen, W. L.; Maxwell, D. S.; Tirado-Rives, J. Development and Testing of the OPLS All-Atom Force Field on Conformational Energetics and Properties of Organic Liquids. *J. Am. Chem. Soc.* **1996**, *118* (45), 11225–11236.

55. Faheem, M.; Heyden, A. Hybrid Quantum Mechanics/Molecular Mechanics Solvation Scheme for Computing Free Energies of Reactions at Metal–Water Interfaces. *J. Chem. Theory Comput.* **2014**, *10* (8), 3354–3368.

56. Burow, A. M.; Sierka, M.; Döbler, J.; Sauer, J. Point Defects in CaF2 and CeO2 Investigated by the Periodic Electrostatic Embedded Cluster Method. *J. Chem. Phys.* **2009**, *130* (17), 174710.

57. Kresse, G.; Hafner, J. Ab initio molecular dynamics for liquid metals. *Phys. Rev. B* **1993**, *47*, 558–561.

58. Kresse, G.; Furthmüller, J. Efficiency of ab-initio total energy calculations for metals and semiconductors using a plane-wave basis set. *Computational Materials Science* **1996**, *6*, 15–50.

59. Kresse, G.; Joubert, D. From ultrasoft pseudopotentials to the projector augmented-wave method. *Phys. Rev. B* **1999**, *59*, 1758–1775.

60. Perdew, J.P.; Wang, Y. Accurate and simple analytic representation of the electron-gas correlation energy. *Phys. Rev. B* **1992**, *45*, 13244–13249.

61. Perdew, J.P.; Yue, W. Accurate and simple density functional for the electronic exchange energy: Generalized gradient approximation. *Phys. Rev. B* **1986**, *33*, 8800–8802.

62. Monkhorst, H. J.; Pack, J. D. Special Points for Brillouin-Zone Integrations. *Phys. Rev. B* **1976**, *13* (12), 5188–5192.

63. Methfessel, M.; Paxton, A. T. High-Precision Sampling for Brillouin-Zone Integration in Metals. *Phys. Rev. B* **1989**, *40* (6), 3616–3621.

64. Piccini, G.; Alessio, M.; Sauer, J. Ab Initio Study of Methanol and Ethanol Adsorption on Brønsted Sites in Zeolite H-MFI. *Phys. Chem. Chem. Phys.* **2018**, *20* (30), 19964–19970.

65. Grimme, S. Supramolecular Binding Thermodynamics by Dispersion-Corrected Density Functional Theory. *Chemistry – A European Journal* **2012**, *18* (32), 9955–9964.

66. Shah, J. K.; Marin-Rimoldi, E.; Mullen, R. G.; Keene, B. P.; Khan, S.; Paluch, A. S.; Rai, N.; Romanielo, L. L.; Rosch, T. W.; Yoo, B.; Maginn, E. J. Cassandra: An Open Source Monte Carlo Package for Molecular Simulation. *Journal of Computational Chemistry* **2017**, *38* (19), 1727–1739

67. Shah, J. K.; Maginn, E. J. A General and Efficient Monte Carlo Method for Sampling Intramolecular Degrees of Freedom of Branched and Cyclic Molecules. *J. Chem. Phys.* **2011**, *135* (13), 134121.

68. Abascal, J. L. F.; Vega, C. A General Purpose Model for the Condensed Phases of Water: TIP4P/2005. *J. Chem. Phys.* **2005**, *123* (23), 234505.

69. Zhu, X.; Riera, M.; Bull-Vulpe, E. F.; Paesani, F. MB-pol(2023): Sub-chemical Accuracy for Water Simulations from the Gas to the Liquid Phase. *Journal of Chemical Theory and Computation* **2023**, *19*, 3551–3566.

70. Saleheen, M.; Heyden, A., Liquid-Phase Modeling in Heterogeneous Catalysis. *ACS Catalysis* **2018,** *8* (3), 2188-2194

71. Faheem, M.; Heyden, A., Hybrid Quantum Mechanics/Molecular Mechanics Solvation Scheme for Computing Free Energies of Reactions at Metal-Water Interfaces. *J Chem Theory Comput* **2014,** *10* (8), 3354-3368

72. Zare, M.; Saleheen, M.; Kundu, S. K.; Heyden, A. Dependency of Solvation Effects on Metal Identity in Surface Reactions. *Commun Chem* **2020**, *3* (1), 1–10.

73. Zare, M.; Saleheen, M. S.; Singh, N.; Uline, M. J.; Faheem, M.; Heyden, A. Liquid-Phase Effects on Adsorption Processes in Heterogeneous Catalysis. *JACS Au* **2022**, *2* (9), 2119–2134.

74. Greydanus, B.; Saleheen, M.; Wu, H.; Heyden, A.; Medline, J. W.; Schwartz, D. K. Probing surface-adsorbate interactions through active particle dynamics. *Journal of Colloid and Interface Science* **2022**, *614*, 425–435.

75. Bennett, C., Efficient Estimation of Free Energy Differences from Monte Carlo Data. *J Comput Phys* **1976,** *22*, 245-268.

76. Reed, A. E.; Weinstock, R. B.; Weinhold, F. Natural Population Analysis. *J. Chem. Phys.* **1985**, *83* (2), 735–746.

77. Zacharias M., Straatsma T. P., McCammon J. A. Separation-shifted scaling, a new scaling method for Lennard-Jones interactions in thermodynamic integration. *The Journal of Chemical Physics* **100**, 9025-9031 (1994).

78. Hunger, B.; Matysik, S.; Heuchel, M.; Einicke, W. D. Adsorption of Methanol on ZSM-5 Zeolites. *Langmuir* **1997**, *13* (23), 6249–6254.

79. Emami, F. S.; Puddu, V.; Berry, R. J.; Varshney, V.; Patwardhan, S. V.; Perry, C. C.; Heinz, H. Force Field and a Surface Model Database for Silica to Simulate Interfacial Properties in Atomic Resolution. *Chem. Mater.* **2014**, *26* (8), 2647–2658.

80. Alexopoulos, K.; Lee, M.-S.; Liu, Y.; Zhi, Y.; Liu, Y.; Reyniers, M.-F.; Marin, G. B.; Glezakou, V.-A.; Rousseau, R.; Lercher, J. A. Anharmonicity and Confinement in Zeolites: Structure, Spectroscopy, and Adsorption Free Energy of Ethanol in H-ZSM-5. *J. Phys. Chem. C* **2016**, *120* (13), 7172–7182.

81. Qiu, X.; Tan, S. P.; Dejam, M.; Adidharma, H. Experimental Study on the Criticality of a Methane/Ethane Mixture Confined in Nanoporous Media. *Langmuir* **2019**, *35* (36), 11635–11642.

82. Tan, S. P.; Qiu, X.; Dejam, M.; Adidharma, H. Critical Point of Fluid Confined in Nanopores: Experimental Detection and Measurement. *J. Phys. Chem. C* **2019**, *123* (15), 9824–9830.

83. Manz, T. A.; Limas, N. G. Introducing DDEC6 Atomic Population Analysis: Part 1. Charge Partitioning Theory and Methodology. *RSC Adv.* **2016**, *6* (53), 47771–47801.

84. Eckstein, S.; Hintermeier, P. H.; Zhao, R.; Baráth, E.; Shi, H.; Liu, Y.; Lercher, J. A. Influence of Hydronium Ions in Zeolites on Sorption. *Angewandte Chemie International Edition* **2019**, *58* (11), 3450–3455.

85. Shi, H.; Eckstein, S.; Vjunov, A.; Camaioni, D. M.; Lercher, J. A. Tailoring Nanoscopic Confines to Maximize Catalytic Activity of Hydronium Ions. *Nat Commun* **2017**, *8* (1), 15442.

86. Hawkins, G. D.; Cramer, C. J.; Truhlar, D. G. Universal Quantum Mechanical Model for Solvation Free Energies Based on Gas-Phase Geometries. *J. Phys. Chem. B* **1998**, *102* (17), 3257–3271.

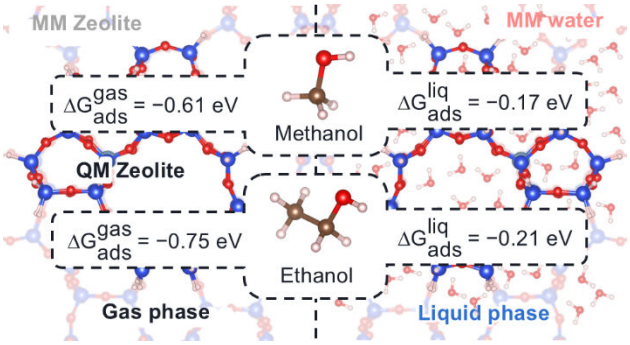

For Table of Contents Only